HHS Public Access

Author manuscript

Int J Orthop (Hong Kong). Author manuscript; available in PMC 2019 February 28.

Published in final edited form as:

Int J Orthop (Hong Kong). 2018 ; 5(1): 863–871.

Finite Element Analysis of the Mouse Distal Femur with Tumor Burden in Response to Knee Loading

Feifei Jiang[1], **Shengzhi Liu**[2,3], **Andy Chen**[2], **Bai-Yan Li**[3], **Alexander G. Robling**[4], **Jie Chen**[1], and **Hiroki Yokota**[1,2,4]

[1]Department of Mechanical Engineering, Indiana University Purdue University Indianapolis, Indianapolis, IN 46202, USA

[2]Department of Biomedical Engineering, Indiana University Purdue University Indianapolis, Indianapolis, IN 46202, USA

[3]Department of Pharmacology, School of Pharmacy, Harbin Medical University, Harbin 150081, China

[4]Department of Anatomy and Cell Biology, Indiana University School of Medicine, Indianapolis, IN 46202, USA

Abstract

Breast cancer-associated bone metastasis induces bone loss, followed by an increased risk of bone fracture. To develop a strategy for preventing tumor growth and protecting bone, an understanding of the mechanical properties of bone under tumor burden is indispensable. Using a mouse model of mammary tumor, we conducted finite element analysis (FEA) of two bone samples from the distal femur. One sample was from a placebo-treated mouse, and the other was from a mouse treated with the investigational drug candidate, PD407824, an inhibitor of checkpoint kinases. Mechanical testing and microCT images revealed that bone strength is improved by administration of PD407824. In response to loading to the knee, FEA predicted that the peaks of von Mises stress, an indicator of fracture yielding, as well as the third principal compressive stress, were higher in the placebo-treated femur than the drug-treated femur. Higher peak stresses in trabecular segments were observed in the lateral condyle, a critical region for integrity of the knee joint. Collectively, this FE study supports the notion that mechanical weakening of the femur was observed in the tumor-invaded trabecular bone, and chemical agents such as PD407824 may potentially assist in preventing bone loss and bone fracture.

Corresponding Author: Hiroki Yokota, PhD, Department of Biomedical Engineering, Indiana University-Purdue University Indianapolis, 723 West Michigan Street, SL220, Indianapolis, IN 46202 USA, Phone: 317-278-5177; Fax: 317-278-2455, hyokota@iupui.edu.

Author contributions

Conception and experimental design: FJ, SL, AC, AR, JC, BL, and HY

Data collection and interpretation: FJ, SL, and AC

Drafted manuscript: FJ, AR, JC, and HY

Competing financial interests

There are no competing financial interests.

Keywords

finite element analysis; bone metastasis; distal femur; knee loading

Introduction

Breast cancer is a serious health problem for women in the U.S. and the rest of the world (1). Tumors at the primary site may be treated surgically or chemically, but they frequently metastasize to other organs, such as the lungs and brain (2). Bone is one of the most frequent sites of metastasis from breast cancer (3). Currently, drugs such as bisphosphonates are administered to reduce bone pain and fracture that are associated with osteolytic reactions in metastasized bone, but there are few treatment options that stop tumor migration and cure bone metastasis (4, 5).

To develop new drugs for suppressing both tumor growth and bone loss, mouse models of mammary tumor and bone metastasis have been employed for testing candidate agents (6). One such drug candidate is everolimus, which is a mammalian target of rapamycin (mTOR) inhibitor (7). Everolimus is approved as an anti-tumor agent for advanced estrogen receptor-positive breast cancer. Another drug candidate is a modulator of dopamine signaling, A77636, which induces apoptosis in tumor cells and inhibits maturation of bone-resorbing osteoclasts (8). We recently examined the effects of inhibitors of checkpoint kinases (Chks), which regulate DNA damage responses and cell cycling, on bone metastasis (9).

In this study, we focused on the effect of PD407824 (10), a selective inhibitor of checkpoint kinase 1 (Chk1), on the distal femur of the mouse knee joint. Activation of Chk1 results in cell cycle arrest, and its mutations are reported to be linked to breast and other cancers (11). Administration of Chk inhibitors for inhibiting tumor growth has been considered (12, 13), and we recently reported the effects of these inhibitors on suppression of bone resorption (14). In this report, we showed that Chk1 inhibitors blocked the proliferation, survival, and migration of tumor cells *in vitro* and suppressed the development of bone-resorbing osteoclasts by downregulating nuclear factor of activated T cells (NFATc1), a master transcription factor for osteoclast development.

The study herein was conducted to characterize the effects of the drug candidate PD407824 on mechanical properties of the mouse distal femur. We first conducted animal experiments and analyzed drug effects using approaches such as X-ray imaging, mechanical testing, microCT imaging, and histology. We then performed FE (finite element) analysis of the distal femur in response to a lateral force applied to the medial side of the condyle, to quantify bone stiffness and strength.

Materials and Methods

Animal model

The experimental procedure was approved by the Indiana University Animal Care and Use Committee and was in compliance with the Guiding Principles in the Care and Use of Animals endorsed by the American Physiological Society. BALB/c female mice were fed

with mouse chow and water *ad libitum*. They received an injection of 4T1.2 mammary tumor cells (1.0×10^5 cells in 50 μl PBS) (15) to the right iliac artery. PD407824 was administered daily via i.p. injection at 2 mg/kg body weight. The animals were sacrificed on day 17. A whole-body X-ray was taken at 25 kV for 10 sec using a Faxitron radiographic system (Faxitron X-ray Corporation) (8), and the femora were harvested for characterization.

Mechanical testing

The whole femur was loaded to failure by four-point bending using a voltage-regulated mechanical loading device (Electro Force 3100, Bose, Inc.), with a loading span of 2.3 mm and a support span of 7 mm (16). Load was applied to the longitudinal center of the diaphysis. After applying a 0.5 N preload, the bone was loaded monotonically at 0.03 mm/s to failure. During bending, displacement and load were recorded to calculate stiffness.

μCT imaging

Micro-computed tomography was performed using a Skyscan 1172 microCT scanner (Bruker-MicroCT, Kontich Belgium) (17). The harvested bone samples were wrapped in parafilm to maintain hydration and placed in a plastic tube and oriented vertically. Scans were performed at pixel size 8.99 μm. Using manufacturer-provided software, the images were reconstructed (nRecon v1.6.9.18).

Histology

Right lower limb specimens were fixed in 10% neutral buffered formalin (Thermo Fisher Scientific) for 48 h and demineralized in 10% EDTA (pH 7.4) at 4°C for three weeks. The samples were dehydrated in graded alcohol and cleared with xylenes (Fisher). Samples were embedded in paraffin, sectioned at 5-μm thicknesses along the sagittal plane, and stained with hematoxylin and eosin for examining metastasized tumor. The nuclei of tumor cells tend to be dyskaryotic and enlarged, and they stained differently with blue-based hematoxylin (8).

Finite element (FE) analysis

FE analysis was conducted using ANSYS workbench 14.5 (ANSYS, Pennsylvania) for two distal femur samples (G1–10 and G6–7). Using microCT images, the medial half of the distal femur was segmented with MIMICS 16 (Materialise, Belgium) and meshed with 3-matic (Materialise, Belgium). We focused on the medial half of distal femur (lateral condyle), which was meshed into ~750,000 tetrahedral elements. The sagittal plane (plane of symmetry) was fixed, and two loading cases were considered: a lateral load of 10 N was applied to the tip of the femur, or the condyle (knee loading). The deformations and stresses resulting from the applied loads were computed.

The average the Hounsfield units (HU) of the placebo and the treated samples were −895.5 and −896.3, respectively. Since differences in HU are negligible between the two samples, the same setting of MIMICS was used to process the CT images of the two femur samples. The HU value is directly related to bone mineral density and Yong's modulus. In this

analysis, we employed Young's modulus of 8.9 GPa and Poisson's ratio of 0.35. The main focus of this study was thus the effect of structural differences in deformation and stress.

Results

Induction of bone metastasis in the mouse model

Metastatic mammary tumor cells were inoculated to mice via the right iliac artery, and invasion of tumor cells in the right hindlimb was induced in two animal groups (10 mice each). According to X-ray imaging, all animals showed induction of bone metastasis in the distal femur. One group was a placebo group that received an equal volume of vehicle, while the other was a PD407824-treated group that received daily injections of an investigational drug agent, PD407824 (Fig. 1A). In FE analysis in this study, we focused on one representative mouse from each treatment group. X-ray images of these two mice on day 17 after inoculation of tumor cells display inflamed muscle around the right femur (Fig. 1B&C). While the PD407824-treated mouse appeared to have denser bone in the distal femur than placebo based on the X-ray's image density, further analysis was needed to evaluate bone quality.

Effects of PD407824 treatment on whole bone strength, trabecular density, and tumor burden

Mechanical testing of the femur using four-point bending showed that compared to the placebo group, the PD407824-treated group showed a significant increase in stiffness ($p = 0.02$). The number of samples was 10 for both groups. Hereafter, we focused on two representative samples. MicroCT imaging and the reconstruction of 3-dimensional structure of these two samples revealed that compared to placebo, the PD407824-treated sample had denser trabecular bone in the distal femur (Fig. 2B). Furthermore, histological analysis using hematoxylin and eosin staining showed that the placebo-treated femur had a region of invaded tumor cells proximal to the growth plate (Fig. 2C). No tumor cells were visible in PD407824-treated sample.

Effects of PD407824 treatment on FE-derived stiffness and von Mises stress

The stiffness of the condyle was determined by displacement in the direction of force application at the loading site, divided by the distance, d, from the loading site to the sagittal plane (Fig. 3). Of note, we used average displacement in local region surrounding loading site and avoided numerical instability due to the stress concentration at the loading site. The predicted stiffness for the two loading cases (BC1 and BC2) are summarized (Tables 1 & 2), while the deformation in the direction of lateral loading is illustrated (Figs. 4 & 5).

Next, we determined the distribution of von Mises stress in two loading cases (Figs. 6 & 7). In both samples, high stresses were predicted in the intercondylar fossa (between medial and lateral condyles). This area was selected for the stress comparison (Table 3). Of note, the high stress at the loading site and the sagittal plane was not analyzed further due to potential uncertainties resulting from stress concentrations and constraints. The failure resistance is characterized by von Mises stress. Since von Mises stress of the PD407824-treated femur

was lower than that of the placebo, the result is in concert with a higher failure resistance of the treated sample.

Effects of PD407824 treatment on third principal stress

Consistent with the predicted von Mises stress, the third principal stress (compressive stress as negative values) presented similar features (Figs. 8 & 9). In response to lateral loading, the placebo sample showed a larger area of high compression (50 MPa or more in the blue zone) at the loading site as well as a wider distribution of high compression in the cross-section. The maximum stress in the intercondylar fossa was compared in two samples (Table 3).

Discussion

This study demonstrates that metastatic invasion of mammary tumor cells to the distal femur reduces local mechanical properties, whereas daily administration of the investigational drug PD407824 prevented metastasis and the consequent reduction in mechanical properties. We employed a mouse model of mammary tumor and bone metastasis in which mammary tumor cells, 4T1.2, were inoculated to the right iliac artery. This tumor cell line is a metastatic triple negative cell line, which is immuno-compatible to BALB/c mice. In response to external loading at 10 N force, which was applied to the lateral condyle, von Mises stress as well as the maximum compressive stress showed peaks at the intercondylar fossa (between medial and lateral condyles). Those peak stresses extended across a wider area in the placebo femur than the PD407824-treated femur, indicating higher stresses in the placebo femur.

The treatment with PD407824 improved both stiffness and strength of the distal femur with higher capacity to withstand loads. MicroCT image analysis revealed that the average HU of the two samples were virtually identical, indicating that a potential change in material properties was negligible. This study was therefore focused on geometric or volumetric changes and their effects on stiffness and stress distributions. The FE analysis revealed that the treatment resulted in a stiffer structure than the untreated placebo. We observed a significant increase in stiffness in the treated sample that produced a >50% decrease in stress. The increase in failure resistance was also demonstrated by reduction in von Mises and maximum compressive stresses.

The predicted mechanical properties by FE analysis are consistent with the experimental results from mechanical testing, microCT imaging, and histological analysis. In FE modeling, the two bone samples had a bone volume of 7.39 mm^3 (placebo) and 9.00 mm^3 (PD407824-treated). Stiffness of the whole femur in four-point bending was 62.37 N/mm (placebo) and 104.12 N/mm (PD407824-treated). Histological analysis together with microCT imaging revealed that the volume of trabecular bone was lower in the placebo sample than the PD407824-treated sample. Of note, the lower volume in placebo was consistent with a region of tumor invasion proximal to the growth plate in the distal femur.

The checkpoint kinase inhibitor PD407824 is an investigational drug candidate that selectively inhibits checkpoint kinase 1 (Chk1) and is being considered for treatment of

various types of cancers. While the effects of Chk1 inhibitors on tumor cells have been reported (18), their role in development of bone-forming osteoblasts and bone-resorbing osteoclasts need to be examined. In our previous study, we conducted *in vitro* and *in vivo* analysis for evaluating the role of PD407824 on MC3T3 osteoblast-like cells as well as RAW264.7 pre-osteoclast cells and found that PD407824 is an effective inhibitor of bone degradation in addition to its anti-tumor effects (14). The current study further supports its potential benefit in preserving bone mechanical properties from degradation by metastatic tumor.

While the present study focused on the distal femur, bone metastasis may occur in other bones, including the spine (19). Bisphosphonates such as zoledronic acid and pamidronate are the standard of care for treating bone metastasis. In future studies, bisphosphonate-treated samples as well as the normal control sample will be compared to the placebo and PD407824-treated samples, and the spine will also be analyzed.

There are limitations in this study. While our FE analysis was focused on two representative bone samples, there are variations in stiffness among animals as shown in Fig. 2A. These variations can be affected not only by efficacy of PD407824 but also size and geometry of individual samples. Of note, the overall weight of animals was not significantly different among the two groups. Although we evaluated the effects of PD407824 in comparison to the placebo sample, the normal control without inoculation of tumor cells presented higher stiffness than the placebo and PD407824-treated samples (data not shown). In summary, this study shows that an integrated analysis using imaging, histological, and FE approaches is useful to comprehensively characterize the mechanical properties of the tumor-invaded bone samples for evaluation of investigational treatment. We found that trabecular bone becomes a target of osteolytic responses that appear to elevate the peak von Mises stress. Future structural characterization of bone metastasis therapies may allow more targeted protection of specific bone types.

Acknowledgments

This study was in part supported by the funds from the breast cancer advocacy group, 100 Voices of Hope, and NIH R01 AR052144 and AR053237.

References

1. Van Poznak CH, Temin S, Yee GC, Janian NA, Barlow WE, Biermann JS, Bosseman LD, Geoghegan C, Hillner BE, Theriault RL, Zuckerman DS, Von Roenn JH. Americal Society of Clinical Oncology. American Society of Clinical Oncology executive summary of the clinical practice guideline update on the role of bone-modifying agents in metastatic breast cancer. J Clin Oncol. 2011; 29:1221–1227. DOI: 10.1200/JCO.2010.32.5209 [PubMed: 21343561]
2. Weigelt B, Peterse JL, van'tVeer LJ. Breast cancer metastasis: markers and models. Nature Rev. 2005; 5:591–602. DOI: 10.1038/nrc1670
3. Roodman G. Mechanisms of bone metastasis. N Engl J Med. 2004; 350:1655–1664. DOI: 10.1056/NEJMra030831 [PubMed: 15084698]
4. Coleman R, Cameron D, Dodwell D, Bell R, Wilson C, Rathbone E, Keane M, Gil M, Burkinshaw R, Grieve R, Barrett-Lee P, Ritchie D, Liversedge V, Hinsley S, Marshall H. AZURE investigators. Adjuvant zoledronic acid in patients with early breast cancer: final efficacy analysis of the AZURE

(BIG 01/04) randomised open-label phase 3 trial. The Lancet Oncology. 2014; 15:997–1006. DOI: 10.1016/S1470-2045(14)70302-X [PubMed: 25035292]

5. Coleman RE. Optimising treatment of bone metastases by Aredia and Zometa. Breast Cancer. 2000; 7:361–369. DOI: 10.1007/bf02966406 [PubMed: 11114866]
6. Wang H, Yu C, Gao X, Welte T, Muscarella AM, Tian L, Zhao H, Zhao Z, Du S, Tao J, Lee B, Westbrook TF, Wong ST, Jin X, Rosen JM, Osborne CK, Zhang XH. The osteogenic niche promotes early-stage bone colonization of disseminated breast cancer cells. Cancer Cell. 2015; 27:193–210. DOI: 10.1016/j.ccell.2014.11.017 [PubMed: 25600338]
7. Squire CJ, Dickson JM, Ivanovic I, Baker EN. Structure and inhibition of the human cell cycle checkpoint kinase, Wee1A kinase: an atypical tyrosine kinase with a key role in CDK1 regulation. Structure. 2005; 13:541–550. DOI: 10.1016/j.str.2004.12.017 [PubMed: 15837193]
8. Minami K, Liu S, Liu Y, Chen A, Wan Q, Na S, Li B-Y, Matsuura N, Koizumi M, Yin Y, Gan L, Xu A, Li J, Nakshatri H, Yokota H. Inhibitory effects of dopamine receptor D1 agonist on mammary tumor and bone metastasis. Scientific Reports. 2017; 7:45686.doi: 10.1038/srep45686 [PubMed: 28374823]
9. Dai Y, Grant S. New insights into checkpoint kinase 1 in the DNA damage response signaling network. Clin Cancer Res. 2010; 16:376–383. DOI: 10.1158/1078-0432.CCR-09-1029 [PubMed: 20068082]
10. Browne AJ, Kubasch ML, Gobel A, Hadji P, Chen D, Rauner M, Stolzel F, Hofbauer LC, Rachner TD. Concurrent antitumor and bone protective effects of everolimus in osteotropic breast cancer. Breast Cancer Res. 2017; 19:92.doi: 10.1186/s13058-017-0885-7 [PubMed: 28793923]
11. Bertoni F, Codegoni AM, Furian D, Tibiletti MG, Capella C, broggini M. CHK1 frame shift mutations in genetically unstable colorectal and endometrial cancers. Genes Chromosomes Cancer. 1999; 26:176–180. DOI: 10.1016/s0959-8049(99)81157-5 [PubMed: 10469457]
12. Sakurikar N, Eastman A. Will targeting Chk1 have a role in the future of cancer treatment? J Clin Oncol. 2015; 33:1075–1077. DOI: 10.1200/JCO.2014.60.0767 [PubMed: 25691674]
13. Rundle S, Bradbury A, Drew Y, Curtin NJ. Targeting the ATR-CHK1 axis in cancer therapy. Cancers. 2017; 9:41.doi: 10.3390/cancers9050041
14. Liu S, Liu Y, Minami K, Chen A, Wan Q, Yin Y, Gan L, Xu A, Matsuura N, Koizumi M, Liu Y, Na S, Li J, Nakshatri H, Li B-Y, Yokota H. Inhibiting checkpoint kinase 1 protects bone from bone resorption by mammary tumor in a mouse model. Oncotarget. 2018; :24286.doi: 10.18632/oncotarget.24286
15. Bolin C, Tawara K, Sutherland C, Redshaw J, Aranda P, Moselhy J, Anderson R, Jorcyk CL. Oncostatin m promotes mammary tumor metastasis to bone and osteolytic bone degradation. Genes Cancer. 2012; 3:117–130. DOI: 10.1177/1947601912458284 [PubMed: 23050044]
16. Collins CJ, Vivanco JF, Sokn SA, Williams BO, Burgers TA, Ploeg HL. Fracture healing in mice lacking Pten in osteoblasts: a micro-computed tomography image-based analysis of the mechanical properties of the femur. J Biomech. 2015; 48:310–317. DOI: 10.1016/j.jbiomech.2014.11.028 [PubMed: 25498366]
17. Wei W, Clockaerts S, Bastiaansen-Jenniskens YM, Gierman LM, Botter SM, Bierma-Zeinstra SM, Weinans H, Verhaar JA, Kloppenburg M, Zuurmond AM, van Osch GJ. Statins and fibrates do not affect development of spontaneous cartilage damage in STR/Ort mice. Osteoarthritis Cartilage. 2014; 22:293–301. DOI: 10.1016/j.joca.2013.11.009 [PubMed: 24280247]
18. McNeely S, Beckmann R, Bence Lin AK. CHEK again: revisiting the development of CHK1 inhibitors for cancer therapy. Pharmacol Ther. 2014; 142:1–10. DOI: 10.1016/j.pharmthera.2013.10.005 [PubMed: 24140082]
19. Ju DG, Yurter A, Gokaslan ZL, Sciubba DM. Diagnosis and surgical management of breast cance metatatic to the spine. World J Clin Oncol. 2014; 5:263–271. DOI: 10.5306/wjco.v5.i3.263 [PubMed: 25114843]

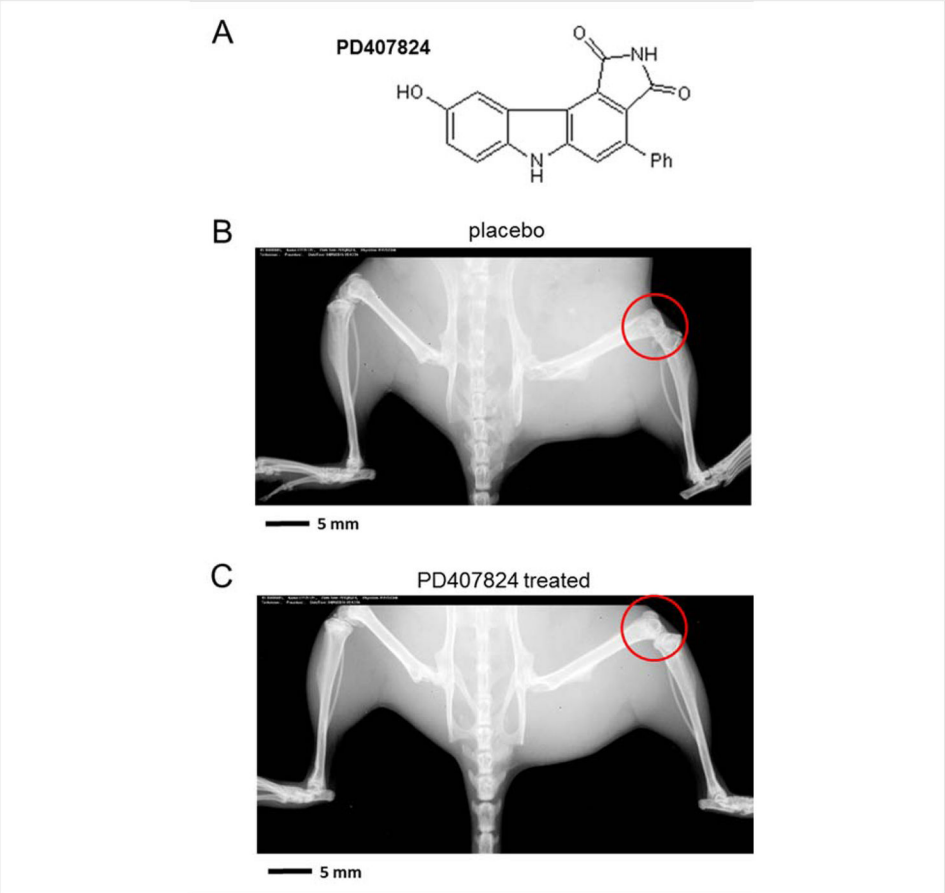

Figure 1.

X-ray images of the placebo and PD407824-treated mice. (A) Chemical structure of PD407824, a selective inhibitor of checkpoint kinase 1. The red circle indicates the distal femur. (B) X-ray image of the placebo mouse (G1–10). (C) X-ray image of PD407824-treated mouse (G6–7). The red circle indicates the distal femur.

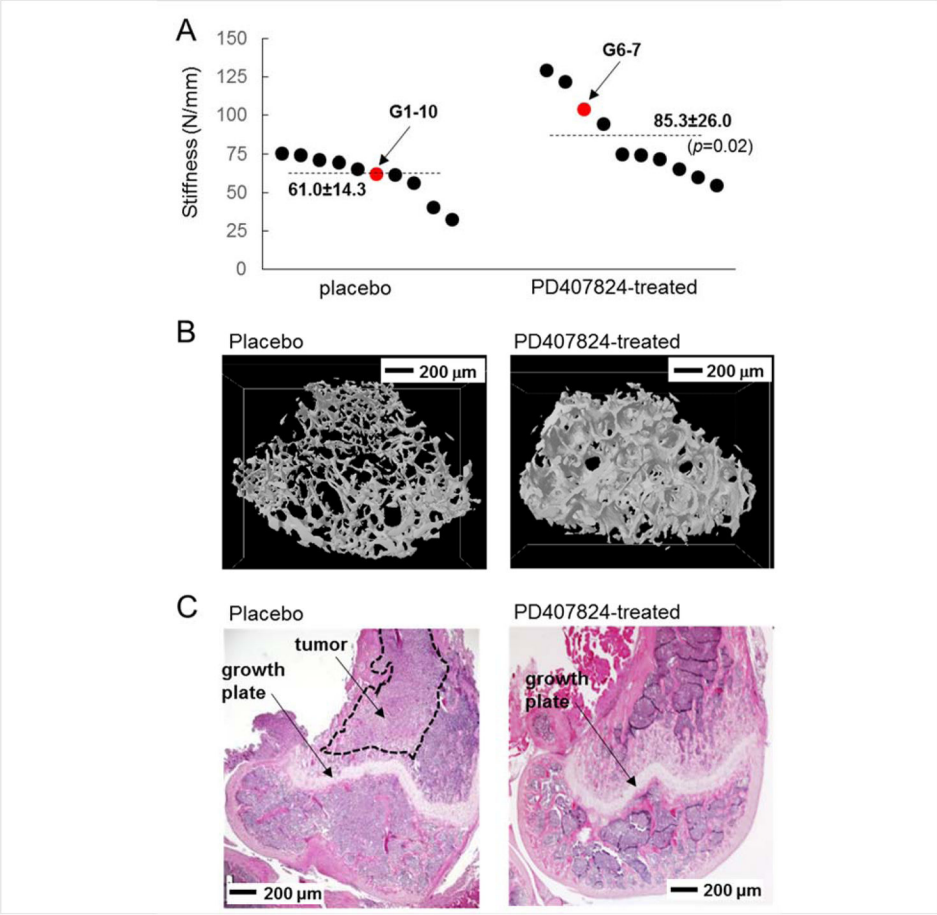

Figure 2.

Mechanical testing, micro CT images, and histology. (A) Stiffness of the femoral shaft using four-point bending. Two samples, employed in this study (G1–10 from the placebo group and G6–7 from the PD407824-treated group), are marked in red. (B) Three-dimensionally reconstructed micro CT images of the distal femur. (C) Hematoxylin and eosin staining of the distal femur. The area, covered by the dotted line in placebo, is invaded with tumor cells.

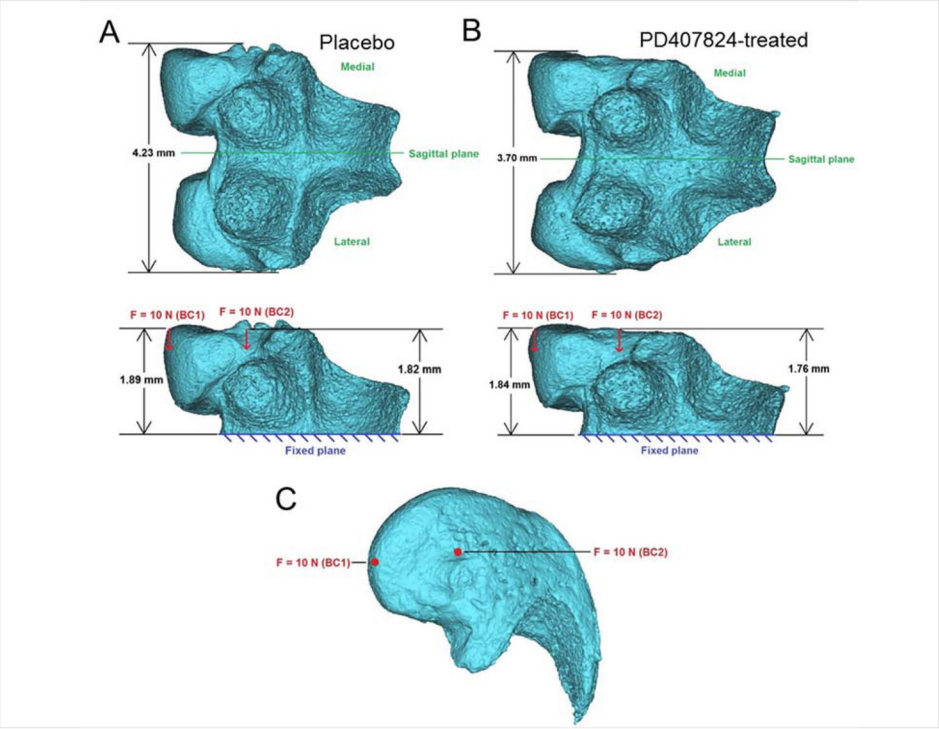

Figure 3.

Location of the two loading sites (BC1 and BC2) on the two distal femurs in this study. (A) Placebo sample. (B) PD407824-treated sample. (C) Loading sites on the condyle from the lateral view.

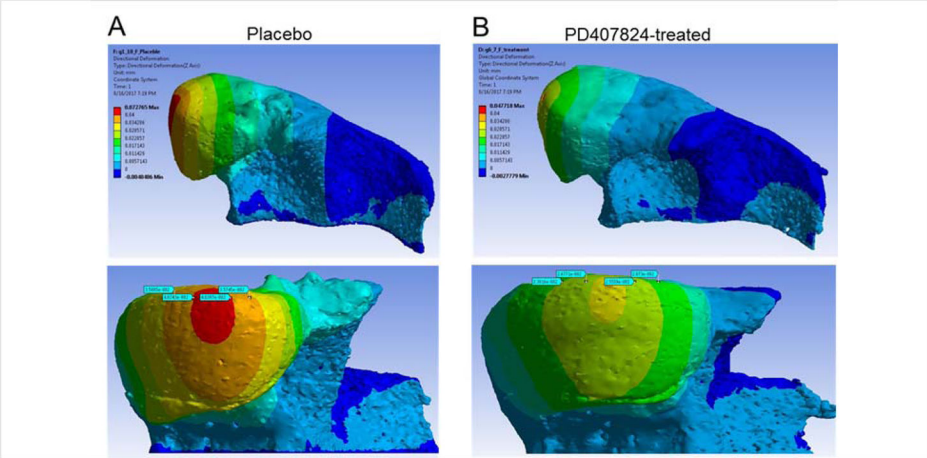

Figure 4.
Deformation in the force direction by lateral loading at the condyle edge (BC1). (A) Placebo sample. (B) PD407824-treated sample.

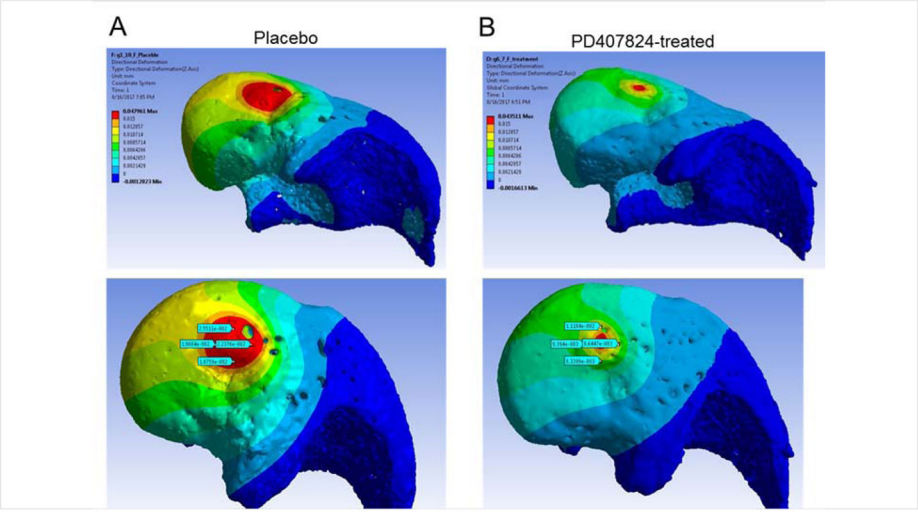

Figure 5.
Deformation in the force direction by lateral loading at the condyle center (BC2). (A) Placebo sample. (B) PD407824-treated sample.

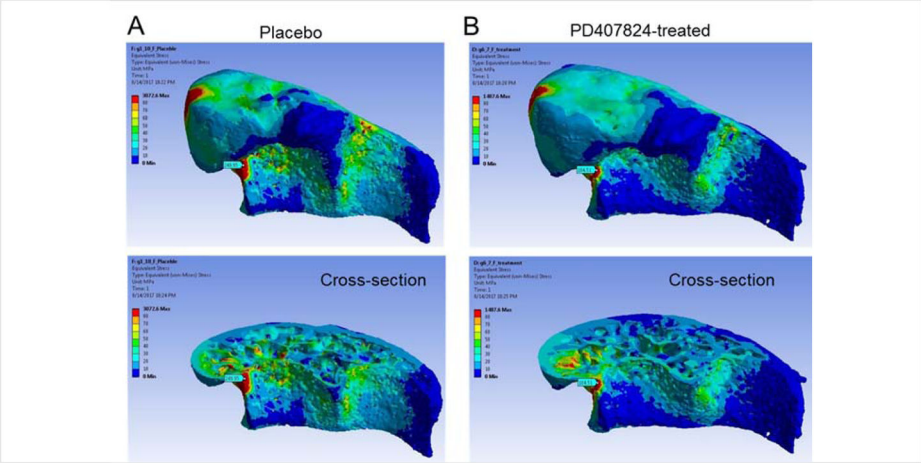

Figure 6.

von-Mises stress in response to lateral loading at the condyle edge (BC1). (A) Surface and cross-sectional stresses of the placebo sample. (B) Surface and cross-sectional stresses of PD407824-treated sample.

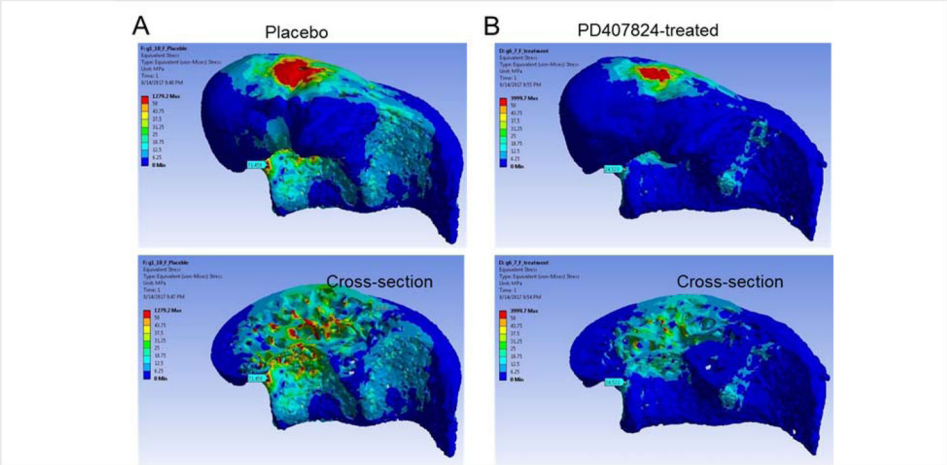

Figure 7.

von-Mises stress in response to lateral loading at the condyle center (BC2). (A) Surface and cross-sectional stresses of the placebo sample. (B) Surface and cross-sectional stresses of PD407824-treated sample.

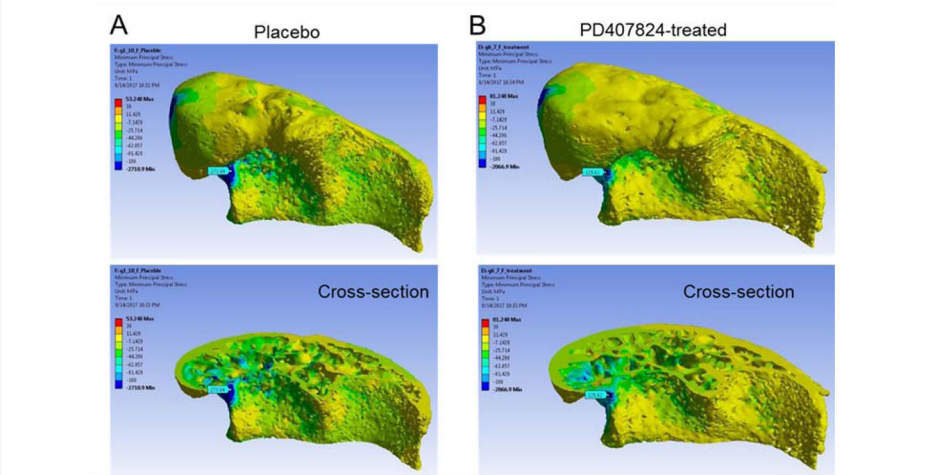

Figure 8.

Third principal stress in response to lateral loading at the condyle edge (BC1). (A) Surface and cross-sectional stresses of the placebo sample. (B) Surface and cross-sectional stresses of PD407824-treated sample.

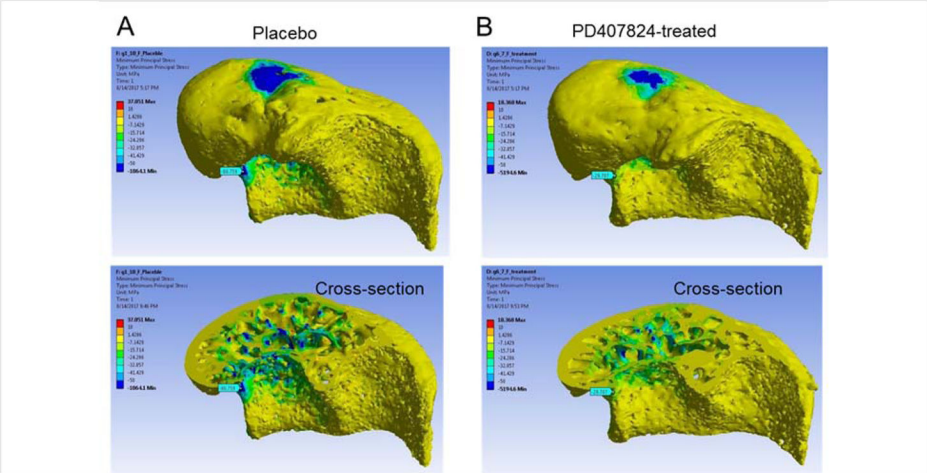

Figure 9.

Third principal stress in response to lateral loading at the condyle center (BC2). (A) Surface and cross-sectional stresses of the placebo sample. (B) Surface and cross-sectional stresses of PD407824-treated sample.

Table 1

Stiffness in response to the loading on the tip.

Sample	*d*	Average displacement	Stiffness
Placebo	1.89 mm	0.040 mm	0.0212
PD407824-treated	1.84 mm	0.027 mm	0.0145

Note: Compared to the placebo femur, the strain of the treated femur decreased 31%.

Table 2

Stiffness in response to the loading on the condyle.

Sample	*d*	Average displacement	Stiffness
Placebo	1.82 mm	0.048 mm	0.0251
PD407824-treated	1.76 mm	0.040 mm	0.0218

Note: Compared to the placebo femur, the strain of the treated femur decreased 53%.

Table 3

Stresses at the intercondylar fossa.

Stress (boundary condition)	Placebo (MPa)	Treated (MPa)	%Decrease
von-Mises stress (BC1)	250	105	58
von-Mises stress (BC2)	71	25	64
3rd principle stress (BC1)	−274	−130	52
3rd principle stress (BC2)	−81	−30	62